X-ray-absorption spectrum of O₂⁺

Lucas M. Cornetta, 1,* Ludvig Kjellsson, 2 Rafael C. Couto, 3 Hans Ågren, 2 Vincenzo Carravetta, 4
Stacey L. Sörensen, 5 Markus Kubin, 6 Christine Bülow, 6 Vicente Zamudio-Bayer, 6 Bernd von Issendorff, 7
J. Tobias Lau, 6,6,7 Johan Söderström, 2 Marcus Agåker, 2 Jan-Erik Rubensson, 2 and Rebecka Lindblad, 6 Instituto de Física, Universidade de São Paulo, Rua do Matão 1731, 05508-090 São Paulo, Brazil
2 Department of Physics and Astronomy, Uppsala University, Box 516, SE-75120 Uppsala, Sweden
3 Department of Chemistry, School of Engineering Sciences in Chemistry, Biotechnology and Health (CBH),

KTH Royal Institute of Technology, SE-10044 Stockholm, Sweden
4 IPCF-CNR, via Moruzzi 1, 56124 Pisa, Italy
5 Department of Physics, Lund University, Lund, Box 118, SE-22100 Lund, Sweden
6 Abteilung für Hochempfindliche Röntgenspektroskopie, Helmholtz-Zentrum Berlin für Materialien und Energie, 12489 Berlin, Germany
7 Physikalisches Institut, Albert-Ludwigs-Universität Freiburg, 79104 Freiburg, Germany

(Received 17 September 2024; accepted 29 January 2025; published 14 February 2025)

The x-ray absorption spectrum of the O_2^+ molecular cation is measured. The ions are stored in a cryogenically cooled radiofrequency ion trap and probed by tunable synchrotron radiation. The spectrum exhibits several salient features: a three-state composite π^* resonance at the low-energy side followed by a two-component exchange split, a highly dissociative, σ^* resonance pulled down well below the ionization limit; and a complex valence-Rydberg high-energy part, including several resolved bands. Small structures are interpreted as correlation state satellites with leading internal or semi-internal configurations. Calculations using the restricted active space wave functions and quantum wave packet dynamics offer an overall excellent interpretation of the spectral features.

DOI: 10.1103/PhysRevA.111.022808

I. INTRODUCTION

The capability to measure high-quality x-ray absorption spectra (XAS) of small molecular ions has generated a lot of new insight in recent years [1-13]. Apart from constituting a new challenge for fundamental molecular theory [14], the results are of relevance in many different fields. First, they provide the reference data needed in ultrafast time-resolved experiments at high-harmonic generation and free-electron laser sources [15,16]. Such data are especially important for attosecond transient absorption spectroscopy [17] where charge migration in molecular ions is investigated, but also for characterizing the background due to transient ionic species that are created in high-intensity experiments [18]. Second, the description of molecular ions is important for modeling plasmas of technical relevance, e.g., in the context of discharges and combustion [19]. Third, molecular ions are of astrophysical interest due to their role in planetary ionospheres [20] and interstellar clouds [21].

As a natural extension of earlier studies of cation near edge x-ray absorption fine-structure (NEXAFS) addressing molecules with a closed shell in their neutral ground states, we here present and analyze the XAS spectrum of a molecule which is open shell in its neutral ground state: molecular

*Contact author: lucas.cornetta@usp.br

oxygen, here measured at the ion trap end-station at the UE52-PGM beamline at the BESSY II synchrotron radiation facility [22,23]. The spectrum was analyzed by means of the restricted active space computational technique for x-ray spectra [24] using implementations [25,26] in the OPENMOL-CAS program suite [27]. In this way it was possible to analyze the effects of relaxation and electron correlation with proper spin coupling. A wavepacket technique was used to characterize the vibrational fine-structure.

Our work reveals several different phenomena with additional insight. The $1s \rightarrow \pi^*$ excitation gives rise to three multiplets with vibrational progressions, similar to the corresponding excitation in the isoelectronic open-shell molecule NO [28]. While the same configuration is populated in corelevel photoemission of the neutral molecule [29], the selection rules lead to a population of states that have not been observed before. The second broad band is also novel in appearance: it is assigned to excitation to two dissociative $1s^{-1}\sigma^*$ states with different internal spin couplings, which, in contrast to the corresponding transitions in the XAS spectrum of neutral O₂, reside well below the ionization limits and are largely separated from Rydberg excitations. Closer to the ionization limits the spectrum exhibits a rich structure, which can be assigned to mixed valence-Rydberg and Rydberg transitions where states with internal and semi-internal excitation patterns can be assigned. The excellent agreement between observations and the predictions of Restricted active space second-order perturbation (RASPT2) theory demonstrates that the specific electron correlation effects associated with cationic XAS [6,10,11] are now fully taken into account.

II. EXPERIMENT

The x-ray absorption spectrum of O_2^+ was measured using synchrotron radiation at the ion trap end-station at the UE52-PGM beamline at the BESSY II synchrotron radiation facility [22]. The same experimental procedure as in our earlier studies [6,7,10,11] was used. Oxygen gas is leaked into a helium plasma, created by magnetron sputtering, where the molecules are excited and ionized. These ions are extracted from the source, O_2^+ ions are selected in a quadrupole mass filter and guided into a cryogenically cooled radiofrequency ion trap. Upon interaction with the synchrotron radiation the ions in the trap are excited and ionized, and the content of the trap is analyzed in a reflectron mass spectrometer. Mass spectra are recorded as the energy of the incident photon energy is varied. Here we assume that the yield of O^+ fragments is proportional to the x-ray absorption cross section of O_2^+ .

The beamline energy was calibrated by a standard procedure using XAS of N_2 [30]. XAS of neutral O_2 was measured using a monochromator exit slit of 15 μ m by electron yield in an upstream gas-cell and used for energy reference. The three regions of the O_2^+ spectrum, 528–565 eV, 530.7–536 eV, 541–558 eV, were each recorded with a different monochromator exit slit. Overview with 100 μ m, high energy with 50 μ m, and the π^* resonance with 15 μ m, correspond to the estimated bandwidths of 130 meV, 70 meV, and 20 meV.

III. THEORY

The simulations of the x-ray absorption spectrum were carried out by a combination of multiconfigurational electronic structure and nuclear wave-packet dynamics methods, in similar fashion as in previous works [6,7,10,11,14]. State-average restricted active space self-consistent field (SA-RASSCF) calculations were performed [24-26], followed by multistate second-order perturbation calculations (MS-RASPT2) [31]. Proper core-valence separation [32,33] restrictions on the O1s core orbitals were imposed to avoid the variational collapse of the wave functions. Preliminary inspections of the XAS structure for O₂⁺ suggest that in the 541 to 558 eV range features below the ionization threshold are characteristic of Rydberg states. Therefore, the ANO-RCC-VQZP basis set was used, together along with an auxiliary Rydberg diffuse basis set for a proper description of such states (Table S1 [34]). For this auxiliary diffuse basis set a $8s8p8d8f \rightarrow [3s2p2d1f]$ contraction scheme is used, in which the primitive functions were obtained from a preset Rydberg basis set proposed by Kaufmann [35]. Since we are dealing with Rydberg states supported by a cationic species, all the exponents in the basis set are multiplied by a factor of 4, $(\alpha \sim Z^2...)$ before the contraction. Scalar relativistic effects are included by using a secondorder Douglas-Kroll-Hess Hamiltonian [36,37], in combination with the atomic natural orbital-RCC (ANO-RCC) basis. Transition dipole moments were obtained by the RAS state-interaction (RASSI) approach [38,39]. Also, the orbitals were localized by the PIPEK-MEZEY procedure [40], and

the calculations were performed at the C_{2v} point group of symmetry. In the RASPT2 step, an imaginary shift of 0.3 Hartree [41] and the default ionization-potential electronaffinity (IPEA) shift of 0.25 Hartree [42] were applied. The potential energy curves were computed considering the active space RAS(13,1,0;1,14,0) active space. The RASSCF active space is labeled RAS(n, l, m; i, j, k), where i, j, and k are the number of orbitals in RAS1, RAS2, and RAS3 spaces, respectively, n is here the total number of electrons in the active space, l the maximum number of holes allowed in RAS1, and m the maximum number of electrons in RAS3. The state-average procedure was performed considering eight states for the π^* region and 20 states for the σ^* and the high-energy region.

The vibrationally resolved spectrum was computed by means of quantum nuclear wave-packet dynamics [43]. The absorption cross section as a function of the incident photon energy (ω) is resolved as the following sum over the excited states:

$$\sigma(\omega) = \operatorname{Re} \sum_{c} \langle \nu_0 | \Psi_c(0) \rangle, \tag{1}$$

where

$$|\Psi_c(0)\rangle = D_{c0} \int_0^\infty e^{i(\omega - \omega_{c0} + \epsilon_{\nu_0} + i\Gamma_c)t} |\psi_c(t)\rangle dt.$$
 (2)

In the above expression, D_{c0} depends on the transition dipole moment between the initial (ground) state and the excited state \mathbf{d}_{c0} and the photon polarization vector \mathbf{e} as in $D_{c0} = (\mathbf{e}\mathbf{d}_{c0})$, ω_{c0} is the vertical transition energy, ϵ_{ν_0} is the vibrational energy of the initial wave packet and Γ_c is the natural width associated with state c. The propagation of the wave packet on each excited state is given by

$$|\psi_c(t)\rangle = e^{-ih_c t} D_{c0} |\nu_0\rangle, \tag{3}$$

where h_c is the nuclear Hamiltonian related to electronic state c. All propagations were addressed within the split-operator technique in a spatial grid in of 2048 points. A total of 2^{18} timesteps was used for the time evolution, with a total time of 10 fs. Equations (1) and (2) were solved with a half-Fourier transform with the use of the fast Fourier transform (FFT) algorithm. The initial wave packet $|\nu_0\rangle$ in all cases was set as the lowest vibrational level of the $^2\Pi$ ground state of O_2^+ . The broadening of the vibrational profile is given by the lifetime broadening of the O_2 core-excited state taken from Coreno et al. [44], which corresponds to $\Gamma=74.7$ meV (half-width at half maximum, HWHM). The spectrum related to each core-excited state was computed separately.

IV. RESULTS AND DISCUSSION

The ground state of the molecular cation O_2^+ is a ${}^2\Pi_g$ multiplet state originating from the $1\sigma_g^21\sigma_u^22\sigma_g^22\sigma_u^23\sigma_g^21\pi_u^41\pi_g^1$ electronic configuration (Fig. S1 [34]). As in earlier XAS investigations of cationic small molecules we find it natural to separately discuss the spectra in the three regions in order of increasing energy: a "repopulation" band associated with filling the vacancy in the outermost orbital of the ion, a composite band of valence excitations, and a series of transitions featuring Rydberg (valence mixing with strong electron

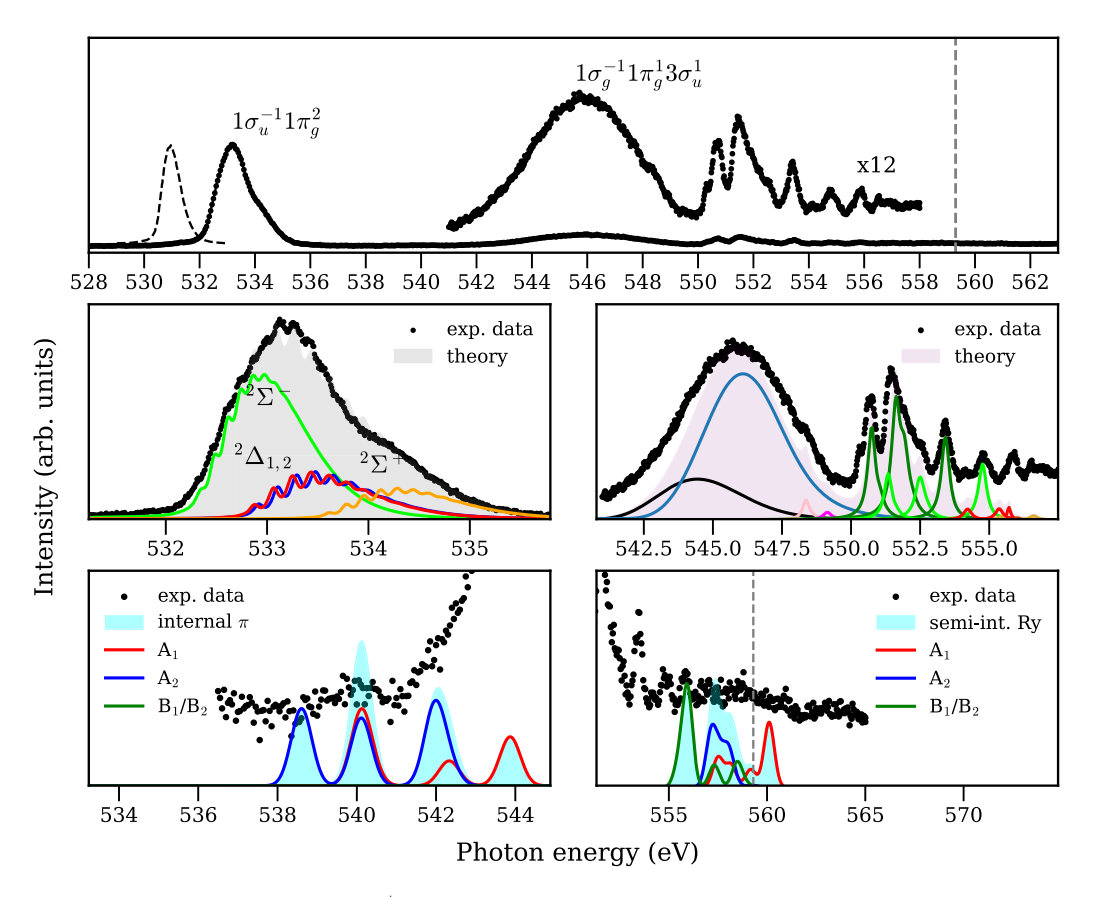


FIG. 1. (Top) The x-ray absorption spectrum of O_2^+ . Neutral O_2 was measured at the O1s- π^* resonance for energy reference and is shown as a dashed line. The threshold for core ionization from the ${}^2\Pi_g$ ground state of the cation to the first ${}^3\Pi_{g,u}$ core-valence states of the dication, marked by a dashed vertical line, is estimated to be at 559.3 eV, by combining valence band [45] and core-valence [46] photoemission. (Middle) Theoretical absorption cross section for the π region (left) and the σ /high-energy region (right), together with the experimental data. The colors of each component of the spectrum respect the color schemes of the potential energy curves shown in Figs. 3 and 4. (Bottom) Transitions related to $\pi_u\pi_g$ (left) and π_u/Ry (right) internal and semi-internal excitations (see text). The theoretical spectra are shifted by -0.31 eV (π^* resonances, middle left), -1.2 eV (σ^* resonances, middle right), and +0.29 eV (Rydberg states: middle right and semi-internal states: bottom).

correlation). The XAS (Fig. 1) spectrum is dominated by a peak that reaches its maximum at 533.2 eV, and can be assigned to transitions to $1\sigma_u^{-1}1\pi_g^{+2}$ states, i.e., the outermost vacancy is filled. O_2^+ is isoelectronic with NO [28,47,48], and we expect qualitatively similar electronic coupling.

The broader feature appearing at 546 eV is the composite valence band, assigned to $1\sigma_g \rightarrow 3\sigma_u$ excitations. As in earlier studies of cationic XAS, the final state in this region has three open shells, the leading configuration being $1\sigma_e 1\pi_e 3\sigma_u$ with the term ${}^{2}\Pi_{u}$. The internal spin coupling splits this state, and the lack of fine-structure indicates that the states are dissociative. The sharp peaks in the 550-558 eV energy range are due to excitations of Rydberg and Rydberg-valence mixed character, and they also involve configurations with double excitations. In addition, we observe weak structures, such that our analysis assigns to internal and semi-internal double excitations, involving the singly occupied $1\pi_g$ orbital. These transitions populate states where $1\sigma_g^{-1}1\pi_u^{-1}1\pi_g^{+2}$ and $1\sigma_g^{-1}1\pi_u^{-1}1\pi_g^{+1}nl^{+1}$ are leading configurations, nl denoting a Rydberg orbital. Such processes become feasible in ionic species with open shells.

Below we discuss these three energy regions in some detail.

A. π^* resonance

The $1\sigma_u \to 1\pi_g$ peak exhibits vibrational fine-structure (Fig. 1, middle left and Fig. 2, bottom) and contributions from several electronic states. In Λ - Σ coupling, the final-state configuration $1\sigma_g^2 1\sigma_u^1 2\sigma_g^2 2\sigma_u^2 3\sigma_g^2 1\pi_u^4 1\pi_g^2$ gives the dipole-allowed terms $^2\Sigma_u^-$, $^2\Delta_u$, and $^2\Sigma_u^+$ (Fig. 3).

It is instructive to compare to x-ray photoemission spectroscopy (XPS) of neutral O2, as the same electronic configuration is reached in both cases. Here the allowed states are ${}^4\Sigma^-_{g/u}$ and ${}^2\Sigma^-_{g/u}$. In the middle panel of Fig 2 the ionization energy of neutral O₂ to the ground state of the ion, measured to be 12.074 eV [45] has been subtracted from the binding energy scale of the XPS spectrum [29] for comparison. It is clear that only the ${}^{2}\Sigma_{u}^{-}$ state is expected to be populated in both spectroscopies. It is immediately obvious that only doublet final states are observed in XAS of the ion, and that vibrational excitations are more prominent than in XPS. Sörensen et al. measured the energy and vibrational constants of the ${}^{2}\Sigma_{\sigma/u}^{-}$ state from the XPS spectra, and theoretically they estimated the gerade-ungerade splitting to be \sim 7 meV [29]. The more extensive vibrational excitations in the NEXAFS case can be understood from the antibonding character of the $1\pi_g$ orbital,

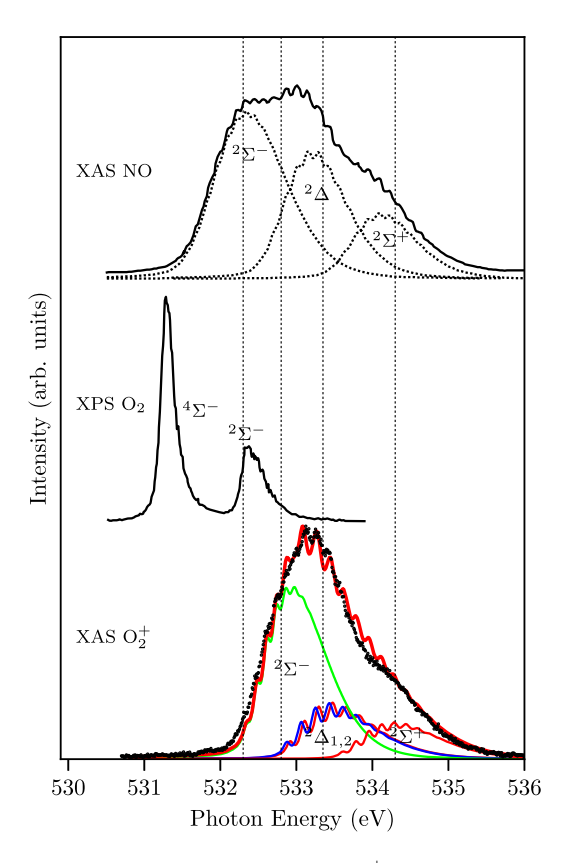


FIG. 2. A comparison between the O_2^+ XAS spectrum at the $1\sigma_u \to 1\pi_g$ resonance (bottom), the XPS spectrum of O_2 [29] (middle), and the O K edge XAS spectrum of NO [28] (top). For comparison, the XPS spectrum is shifted by subtracting the valence ionization energy [45] from the measured binding energy scale.

the population of which gives an additional bond extension compared to the opening of the bare oxygen core orbital [49].

In oxygen K edge XAS of the NO the ${}^2\Sigma_u^-, {}^2\Delta_u$, and ${}^2\Sigma_u^+$ final states give rise to a structured peak including vibrational excitations (Fig. 2, top), which has been thoroughly analyzed [28,48]. The comparison between the spectra of NO and O_2^+ is motivated by their similar electronic configuration, term-designation, and mass. Indeed, the $1\sigma_u \to 1\pi_g$ resonance in O_2^+ and NO (Fig. 2) has a similar shape, with a threefold structure, although the O_2^+ peak appears at higher energy, is

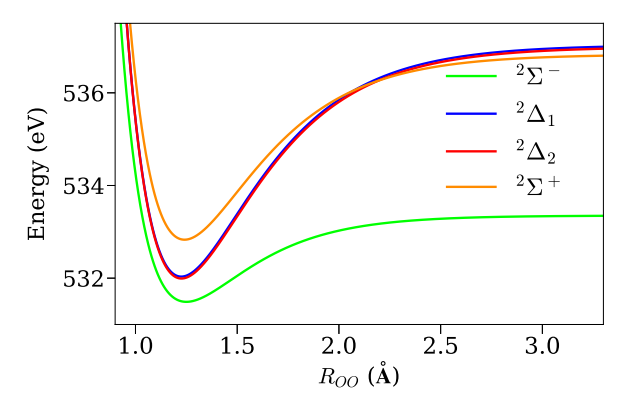


FIG. 3. Potential energy curves, in eV, for the first four core-excited states of O_2^+ .

TABLE I. Theoretical molecular constants for O_2^+ . E_{00} stands for the potential energy minimum in relation to the ground-state minimum, R_e is the equilibrium bond length, ω_e denotes the harmonic frequency, and $\omega_e \chi_e$ is the anharmonicity constant.

State	E ₀₀ [eV]	R_e [Å]	ω_e [meV]	$\omega_e \chi_e \text{ [meV]}$
Ground state	-	1.118	234.5	2.1
$^2\Sigma^-$	531.49	1.250	140.2	2.6
$^{2}\Delta$	531.99	1.226	192.1	1.8
$^{2}\Delta$	532.03	1.225	192.5	1.9
$2\sum_{}^{+}$	532.83	1.241	176.4	1.9

narrower than its NO counterpart, and the vibrational finestructure is not as clearly resolved.

The theoretical prediction (Fig. 1, middle left and Fig. 2, bottom) is in excellent agreement with the observed peak shape. It confirms that the ordering of the ${}^2\Sigma_u^-$, ${}^2\Delta_u$, and ${}^2\Sigma_u^+$ final states are the same as in the NO counterpart, and it gives two close-lying spin-orbit components of the ${}^2\Delta_u$ term. We see a large number of vibrational excitations in both the NO and O_2^+ spectra, and the similarities suggest that the $1\sigma_u \to 1\pi_g$ excitation leads to a similar bond elongation in the two cases. In Table I we list the theoretical constants for the observed states. Although it is difficult to extract the corresponding experimental values from the spectra, the overall agreement (Fig. 2) corroborates the theoretical values.

Finally, we compare the energy split due to π^2 coupling in three cases. Close to the ${}^3\Sigma_g^-$ ground state of neutral O_2 , we find the two excited singlet-oxygen states, ${}^1\Delta_g$ and ${}^1\Sigma_g^+$. In the core-excited doublet states of O_2^+ , the three states directly correspond to the ${}^2\Sigma_u^-$, ${}^2\Delta_u$, and ${}^2\Sigma_u^+$ states, where the only difference is due to the core hole. We note that the ${}^3\Sigma_g^-$ - ${}^1\Delta_g$ and the ${}^3\Sigma_g^-$ - ${}^1\Sigma_g^+$ separations close to the O_2 ground state are 1.0 eV, and 1.64 eV, respectively [50], while the corresponding values for core-excited O_2^+ are calculated to be 0.7 eV, and 1.6 eV. The similarity suggests that the extra unpaired core-electron contributes very little to the valence coupling, and that relaxation due to the core hole is of less importance. In line with the comparison in Fig. 2, the separation between the states in NO is somewhat larger, 1.1 eV and 2.0 eV for the ${}^3\Sigma_g^-$ - ${}^1\Delta_g$ and ${}^3\Sigma_g^-$ - ${}^1\Sigma_g^+$ separations, respectively [28].

B. σ^* resonance

We assign the broad feature at around 546 eV (Fig. 1) to the $1\sigma_g \to 3\sigma_u$ resonance, and thus to the ${}^2\Pi_u$ final state of the $1\sigma_g^1 1\sigma_u^2 2\sigma_g^2 2\sigma_u^2 3\sigma_g^2 1\pi_u^4 1\pi_g^1 3\sigma_u^1$ configuration. For small molecules, this so-called σ^* resonance is generally situated in the continuum, often forming a shape resonance, or lying close to the ionization limit. In neutral O_2 , the valence excited state interacts and overlaps with Rydberg states creating a complex spectral structure [51–53]. In the case of O_2^+ the σ^* resonance is pulled deeply below the ionization limit, and is well separated from the Rydberg excitations. This is attributed to the stronger positive potential for the σ^* state in the ion. The width of the peak and its lack of fine-structure is inline with the expectation that the state is dissociative. We show below that the unresolved structure comprises two

states with two different internal spin-coupling involving the open shells, like in the neutral counterpart [51,52] and in the XAS of other diatomic ions [6,7]. The appearance of the σ^* resonance can also be qualified in light of earlier analysis of cationic NEXAFS spectra involving valence levels where these transitions are quite well described in an "extended one-electron picture" or a picture referring to the smallest possible linear combination of determinants that fulfill spatial and spin symmetry [10,11]. Exchange interaction between the open shell orbitals serves as the main source for the energy splitting, where this interaction between valence highest occupied molecular orbital (HOMO) and lowest unoccupied molecular orbital (LUMO) shells is generally stronger than that between core and any of these shells. The spatial distribution of the HOMO and LUMO orbitals is found to strongly dictate both the energy splitting and relative intensities. The potential curves for the two spin-coupled states are in general quite different (Fig. 4), resulting in widely different vibrational progressions [10,11]. Inspecting the computational results for O_2^+ we see similar features for the spin-coupled valence transitions, although in this case we have an open-shell ground state and valence level of σ^* character (instead of π^*), which, moreover, is strongly dissociative compared to the π^* states in N_2 and CO. Based on the excellent agreement with the predicted σ^* band shape, we can conclude that the splitting between the vertical energies for the two spin-components is about 2.5 eV and where the intensity of the upper component is dominant. The subtle dependence on exchange interaction dictates the final outcome, something that is well reproduced by the RAS calculations.

C. High-energy correlation-state transitions

Earlier recordings of the "third part" of cationic XAS spectra have shown wide, very irregular, but sharp, features. In

contrast to neutral molecular XAS there is no or little indication of Rydberg series or mixed valence-Rydberg transitions. N_2^+ and CO^+ are perhaps the best examples exhibiting well defined spectroscopic features in this high energy part [6,7]. There are a couple of reasons for this. One is that many of the correlated, two-electron two-hole transitions that appear above the ionization threshold in neutral molecules [54] are pulled down below the IP by the stronger potential of the cation where they mix with the Rydberg states. A number of such transitions with multiconfigurational character were assigned by MS-RASPT2 calculations in the previous works on N_2^+ and CO^+ [6,7].

A second reason for the appearance of distinct multielectron states in the upper part of the spectra is that with an open valence shell in the initial state so-called semi-internal transitions can come into play. These are defined as double excitations involving an internal excitation (occupied to partly occupied orbital) coupled to an external excitation (occupied to unoccupied orbital). Such transitions are also important in the inner parts of XPS or UPS [55] spectra and in large parts of valence Auger spectra [56,57] as well as in related processes like the intermolecular Coulombic decay (ICD) effect [58]. It leads to the breakdown of the molecular orbital picture implying that a one-to-one mapping between orbitals and transitions is no longer possible, or expressed differently, a certain one-particle transition appears in more than one state. In the spectra of N_2^+ [6], CO^+ [7], and NO^+ [11] many of states mixed with semi-internal transitions were predicted and observed, but with somewhat different appearance. "Normal" transitions to states having a dominating one-electron excitation with the singly occupied MO as spectator were also predicted in these spectra.

In light of these earlier findings it is interesting to inspect the energies, intensities, and the dominant configurations of

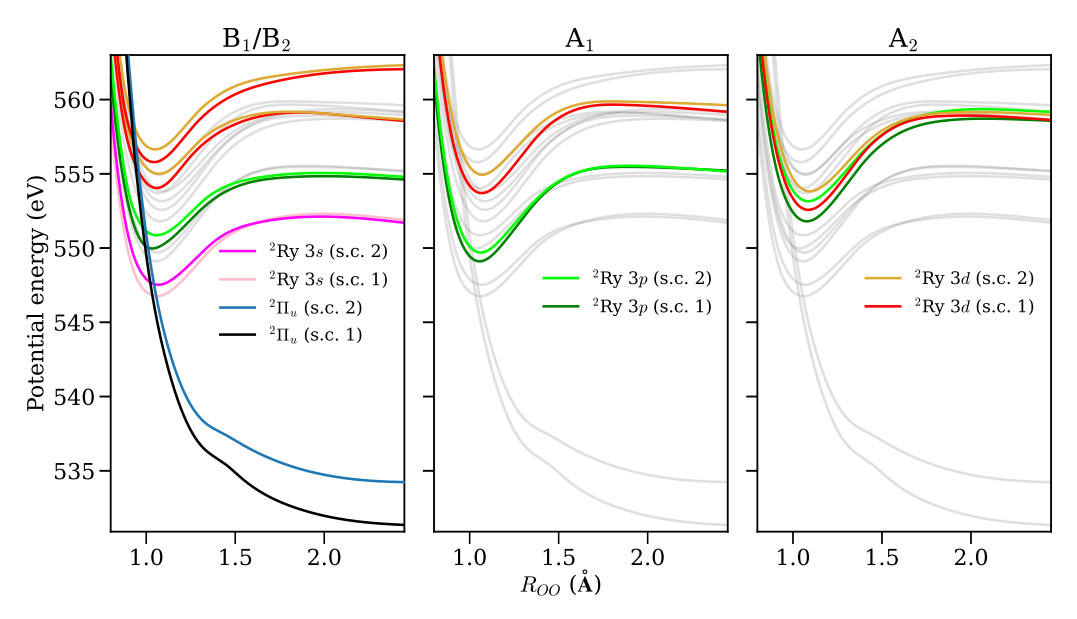


FIG. 4. Potential energy curves, in eV, for the dissociative ${}^2\Pi_u$ resonance $(1\sigma_g^{-1}\pi_g^13\sigma_u^1)$ and for the first Rydberg states. The panels are divided by the symmetry of the electronic wave function of the cation, namely, B_1/B_2 (left), A_1 (middle), A_2 (right), and components. The s.c. notation in the label stands for different spin couplings of the doublet states (see text). The color scheme follows the nature of the state, with σ^* (blue and black lines on the B_1/B_2 panel), $1\sigma^{-1}\pi_g^13s^1$ (Ry) (pink and magenta: two states), $1\sigma^{-1}\pi_g^13p^1$ (Ry) (green and lime: six states), and $1\sigma^{-1}\pi_g^13d^1$ (Ry) (yellow: eight states). The energy scale is referenced at the O_2^+ ground-state energy at the equilibrium geometry.

the transitions of the upper part of the O_2^+ XAS spectrum. These transitions appear with quite high, and irregular, relative intensity. Assignments indicate their Rydberg nature with some configuration mixing. They also appear considerably broadened as confirmed by the vibrational analysis, something that further supports their valence mixing character. In the O_2^+ case we predict that the semi-internals not only mix with Rydberg excitation, but also that groups of states appear where the semi-internals are the configurations with the largest squared coefficients, thus dominating the wave functions. The calculations predict these states are at 555–560 eV at the high-energy side of the Rydberg transitions, where they probably refer to the faint structures observed in that range. They are assigned as coupled internal (mostly π to π^*) and external core to Rydberg orbital excitations. However, there is also a group of transitions predicted to be below the σ^* at 537–542 eV, this group comprises internal excitations, actually double internal excitations, where a π to π^* excitation is coupled to the core π^* excitation.

V. CONCLUSION

We presented and analyzed the XAS spectrum of O_2^+ . Overall the spectrum presents some salient differences with respect to earlier recorded XAS spectra of molecular ions. The π^* excitation comprises three states with different coupling due to the open shell with two π_g electrons in the final state. The splitting between the states is smaller than in the corresponding resonance in isoelectronic NO, a difference which can be attributed to differences in the spatial distribution of the π orbitals. A broad spectral feature is assigned to the σ^* resonance, which is located well below the ionization limit and

seemingly separated from sharper Rydberg features. It comprises two steeply dissociative states with identical electronic configuration split by their different spin coupling schemes by an amount that is determined by the exchange interaction between the two open shells. At higher energies we find complex structures which are assigned to states with mixed configurations including excitations to Rydberg states. Two groups of weak features in the high-energy part of the spectrum are assigned to electron correlation states with leading internal, respectively, semi-internal configurations. The spectrum was analyzed by the RASPT2 computational method, leading to excellent agreement with the experiment which in turn made it possible to confidently assign the spectrum.

ACKNOWLEDGMENTS

Beamtime for this project was granted at the IonTrap station of the UE52-PGM beamline at the BESSY II electron storage ring operated by the Helmholtz-Zentrum Berlin für Materialien und Energie. This project received funding from the European Union's Horizon 2020 research and innovation program under Grant Agreement No. 730872 and by the German Federal Ministry of Education and Research (BMBF) through Grant No. BMBF-05K16Vf2. L.M.C. acknowledges the Brazilian funding agency FAPESP under Grant No. 2021/06527-7. R.L., J.-E.R., and H.A. acknowledge funding from the Swedish Research Council, Contracts No. 637-2014-6929, No. 2021-04017, and No. 2022-03405, respectively. The authors thank the National Academic Infrastructure for Supercomputing in Sweden (NAISS) at the National Supercomputer Centre of Linköping University partially funded by the Swedish Research Council through Grant Agreement No. 2022-06725.

- [1] J.-P. Mosnier, E. T. Kennedy, P. van Kampen, D. Cubaynes, S. Guilbaud, N. Sisourat, A. Puglisi, S. Carniato, and J.-M. Bizau, Inner-shell photoexcitations as probes of the molecular ions CH⁺, OH⁺, and SiH⁺: Measurements and theory, Phys. Rev. A 93, 061401(R) (2016).
- [2] S. Klumpp, A. A. Guda, K. Schubert, K. Mertens, J. Hellhund, A. Müller, S. Schippers, S. Bari, and M. Martins, Photoabsorption of the molecular IH cation at the iodine 3d absorption edge, Phys. Rev. A 97, 033401 (2018).
- [3] S. Bari, L. Inhester, K. Schubert, K. Mertens, J. O. Schunck, S. Dörner, S. Deinert, L. Schwob, S. Schippers, A. Müller, S. Klumpp, and M. Martins, Inner-shell x-ray absorption spectra of the cationic series NH_y⁺(y = 0-3), Phys. Chem. Chem. Phys. 21, 16505 (2019).
- [4] K. Schubert, A. A. Guda, K. Mertens, J. O. Schunck, S. Schippers, A. Müller, S. Bari, S. Klumpp, and M. Martins, Absorption spectra at the iodine 3d ionisation threshold following the $CH_xI^+(x=0-3)$ cation sequence, Phys. Chem. Chem. Phys. **21**, 25415 (2019).
- [5] E. T. Kennedy, J. P. Mosnier, P. V. Kampen, J. M. Bizau, D. Cubaynes, S. Guilbaud, S. Carniato, A. Puglisi, and N. Sisourat, Vibrational effects in the photo-ion yield spectrum of the SiH₂⁺

- molecular ion following 2p inner-shell excitation, J. Phys.: Conf. Ser. **1289**, 012003 (2019).
- [6] R. Lindblad, L. Kjellsson, R. C. Couto, M. Timm, C. Bülow, V. Zamudio-Bayer, M. Lundberg, B. von Issendorff, J. T. Lau, S. L. Sorensen, V. Carravetta, H. Ågren, and J.-E. Rubensson, X-ray absorption spectrum of the N₂⁺ molecular ion, Phys. Rev. Lett. 124, 203001 (2020).
- [7] R. C. Couto, L. Kjellsson, H. Ågren, V. Carravetta, S. L. Sorensen, M. Kubin, C. Bülow, M. Timm, V. Zamudio-Bayer, B. Von Issendorff, J. T. Lau, J. Söderström, J.-E. Rubensson, and R. Lindblad, The carbon and oxygen K-edge nexafs spectra of CO⁺, Phys. Chem. Chem. Phys. 22, 16215 (2020).
- [8] S. Carniato, J.-M. Bizau, D. Cubaynes, E. T. Kennedy, S. Guilbaud, E. Sokell, B. McLaughlin, and J.-P. Mosnier, Vibrationally and spin-orbit-resolved inner-shell x-ray absorption spectroscopy of the NH⁺ molecular ion: Measurements and *ab initio* calculations, Atoms 8, 67 (2020).
- [9] M. Martins, S. Reinwardt, J. O. Schunck, J. Schwarz, K. Baev, A. Müller, T. Buhr, A. Perry-Sassmannshausen, S. Klumpp, and S. Schippers, Disentangling the photodissociation dynamics of the HF⁺ molecular radical via kinetic-energy-release-resolved

- F 1s core excitation and ionization, J. Phys. Chem. Lett. 12, 1390 (2021).
- [10] R. C. Couto, W. Hua, R. Lindblad, L. Kjellsson, S. L. Sorensen, M. Kubin, C. Bülow, M. Timm, V. Zamudio-Bayer, B. von Issendorff, J. Söderström, J. T. Lau, J.-E. Rubensson, H. Ågren, and V. Carravetta, Breaking inversion symmetry by protonation: experimental and theoretical NEXAFS study of the diazynium ion, N₂H⁺, Phys. Chem. Chem. Phys. 23, 17166 (2021).
- [11] R. Lindblad, L. Kjellsson, E. De Santis, V. Zamudio-Bayer, B. von Issendorff, S. L. Sorensen, J. T. Lau, W. Hua, V. Carravetta, J.-E. Rubensson, H. Ågren, and R. C. Couto, Experimental and theoretical near-edge x-ray-absorption fine-structure studies of NO⁺, Phys. Rev. A 106, 042814 (2022).
- [12] J. Schwarz, F. Kielgast, I. Baev, S. Reinwardt, F. Trinter, S. Klumpp, A. Perry-Sassmannshausen, T. Buhr, S. Schippers, A. Müller, S. Bari, V. Mondes, R. Flesch, E. Rühl, and M. Martins, X-ray absorption spectroscopy of H₃O⁺, Phys. Chem. Chem. Phys. 24, 23119 (2022).
- [13] S. Schippers, P.-M. Hillenbrand, A. Perry-Sassmannshausen, T. Buhr, S. Fuchs, S. Reinwardt, F. Trinter, A. Müller, and M. Martins, Vibrationally resolved inner-shell photoexcitation of the molecular anion C₂⁻, ChemPhysChem 24, e202300061 (2023).
- [14] V. Carravetta, R. C. Couto, and H. Ågren, X-ray absorption of molecular cations—a new challenge for electronic structure theory, J. Phys.: Condens. Matter **34**, 363002 (2022).
- [15] L. Young, K. Ueda, M. Gühr, P. H. Bucksbaum, M. Simon, S. Mukamel, N. Rohringer, K. C. Prince, C. Masciovecchio, M. Meyer, A. Rudenko, D. Rolles, C. Bostedt, M. Fuchs, D. A. Reis, R. Santra, H. Kapteyn, M. Murnane, H. Ibrahim, F. Légaré et al., Roadmap of ultrafast x-ray atomic and molecular physics, J. Phys. B: At. Mol. Opt. Phys. 51, 032003 (2018).
- [16] M. Chergui, M. Beye, S. Mukamel, C. Svetina, and C. Masciovecchio, Progress and prospects in nonlinear extreme-ultraviolet and x-ray optics and spectroscopy, Nat. Rev. Phys. 5, 578 (2023).
- [17] C. H. Yuen and C. D. Lin, Quantifying robustness of attosecond transient absorption spectroscopy for vibronic coherence in charge migration, arXiv:2307.13819.
- [18] V. Kimberg, A. Sanchez-Gonzalez, L. Mercadier, C. Weninger, A. Lutman, D. Ratner, R. Coffee, M. Bucher, M. Mucke, M. Agåker, C. Såthe, C. Bostedt, J. Nordgren, J. E. Rubenssone, and N. Rohringer, Stimulated x-ray Raman scattering—a critical assessment of the building block of nonlinear x-ray spectroscopy, Faraday Discuss. 194, 305 (2016).
- [19] N. L. Aleksandrov, E. M. Bazelyan, A. A. Ponomarev, and A. Y. Starikovsky, Kinetics of charged species in non-equilibrium plasma in water vapor- and hydrocarbon-containing gaseous mixtures, J. Phys. D 55, 383002 (2022).
- [20] N. S. Shuman, D. E. Hunton, and A. A. Viggiano, Ambient and modified atmospheric ion chemistry: From top to bottom, Chem. Rev. **115**, 4542 (2015).
- [21] T. P. Snow and V. M. Bierbaum, Ion chemistry in the interstellar medium, Annu. Rev. Anal. Chem. 1, 229 (2008).
- [22] K. Hirsch, J. T. Lau, P. Klar, A. Langenberg, J. Probst, J. Rittmann, M. Vogel, V. Zamudio-Bayer, T. Möller, and B. von Issendorff, X-ray spectroscopy on size-selected clusters in an ion trap: from the molecular limit to bulk properties, J. Phys. B 42, 154029 (2009).

- [23] R. Ovsyannikov and T. Lau, The variable polarization undulator beamline UE₅₂ PGM nanocluster trap at BESSY II, J. Large Scale Res. Facil. JLSRF 3, A105 (2017).
- [24] H. Ågren, A. Flores-Riveros, and H. Jensen, An efficient method for calculating molecular radiative intensities in the VUV and soft x-ray wavelength regions, Phys. Scr. 40, 745 (1989).
- [25] H. J. A. Jensen, P. Jørgensen, and H. Ågren, Efficient optimization of large scale MCSCF wave functions with a restricted step algorithm, J. Chem. Phys. 87, 451 (1987).
- [26] P. Å. Malmqvist, A. Rendell, and B. O. Roos, The restricted active space self-consistent-field method, implemented with a split graph unitary group approach, J. Phys. Chem. 94, 5477 (1990).
- [27] G. Li Manni, I. Fdez. Galván, A. Alavi, F. Aleotti, F. Aquilante, J. Autschbach, D. Avagliano, A. Baiardi, J. J. Bao, S. Battaglia, L. Birnoschi, A. Blanco-González, S. I. Bokarev, R. Broer, R. Cacciari, P. B. Calio, R. K. Carlson, R. Carvalho Couto, L. Cerdán, L. F. Chibotaru *et al.*, The OpenMolcas *Web*: A community-driven approach to advancing computational chemistry, J. Chem. Theory Comput. 19, 6933 (2023).
- [28] R. Püttner, I. Dominguez, T. J. Morgan, C. Cisneros, R. F. Fink, E. Rotenberg, T. Warwick, M. Domke, G. Kaindl, and A. S. Schlachter, Vibrationally resolved O 1s core-excitation spectra of CO and NO, Phys. Rev. A 59, 3415 (1999).
- [29] S. Sorensen, K. Børve, R. Feifel, A. De Fanis, and K. Ueda, The O 1s photoelectron spectrum of molecular oxygen revisited, J. Phys. B: At. Mol. Opt. Phys. 41, 095101 (2008).
- [30] M. R. Weiss, R. Follath, K. J. S. Sawhney, and T. Zeschke, Absolute energy calibration for plane grating monochromators, Nucl. Instrum. Methods Phys. Res. Sect. A 467-468, 482 (2001).
- [31] P. Å. Malmqvist, K. Pierloot, A. R. M. Shahi, C. J. Cramer, and L. Gagliardi, The restricted active space followed by secondorder perturbation theory method: Theory and application to the study of Cu O₂ and Cu₂ O₂ systems, J. Chem. Phys. 128, 204109 (2008).
- [32] L. S. Cederbaum, W. Domcke, and J. Schirmer, Many-body theory of core holes, Phys. Rev. A 22, 206 (1980).
- [33] M. G. Delcey, L. K. Sørensen, M. Vacher, R. C. Couto, and M. Lundberg, Efficient calculations of a large number of highly excited states for multiconfigurational wavefunctions, J. Comput. Chem. 40, 1789 (2019).
- [34] See Supplemental Material at http://link.aps.org/supplemental/ 10.1103/PhysRevA.111.022808 for numerical parameters of the additional basis set used in the quantum chemical calculations, a molecular orbital diagram, and for oscillator strengths of some relevant excitations..
- [35] K. Kaufmann, W. Baumeister, and M. Jungen, Universal Gaussian basis sets for an optimum representation of Rydberg and continuum wavefunctions, J. Phys. B: At. Mol. Opt. Phys. 22, 2223 (1989).
- [36] M. Douglas and N. M. Kroll, Quantum electrodynamical corrections to the fine structure of helium, Ann. Phys. (NY) 82, 89 (1974).
- [37] B. A. Hess, Relativistic electronic-structure calculations employing a two-component no-pair formalism with external-field projection operators, Phys. Rev. A 33, 3742 (1986).
- [38] P.-Å. Malmqvist and B. O. Roos, The CASSCF state interaction method, Chem. Phys. Lett. 155, 189 (1989).

- [39] P. Å. Malmqvist, B. O. Roos, and B. Schimmelpfennig, The restricted active space (RAS) state interaction approach with spin-orbit coupling, Chem. Phys. Lett. **357**, 230 (2002).
- [40] J. Pipek and P. G. Mezey, A fast intrinsic localization procedure applicable for *ab initio* and semiempirical linear combination of atomic orbital wave functions, J. Chem. Phys. **90**, 4916 (1989).
- [41] N. Forsberg and P.-Å. Malmqvist, Multiconfiguration perturbation theory with imaginary level shift, Chem. Phys. Lett. 274, 196 (1997).
- [42] G. Ghigo, B. O. Roos, and P.-Å. Malmqvist, A modified definition of the zeroth-order Hamiltonian in multiconfigurational perturbation theory (CASPT2), Chem. Phys. Lett. 396, 142 (2004).
- [43] F. Gel'mukhanov and H. Ågren, Resonant x-ray Raman scattering, Phys. Rep. **312**, 87 (1999).
- [44] M. Coreno, M. de Simone, K. Prince, R. Richter, M. Vondráček, L. Avaldi, and R. Camilloni, Vibrationally resolved oxygen K → Π* spectra of O₂ and CO, Chem. Phys. Lett. 306, 269 (1999).
- [45] P. Baltzer, B. Wannberg, L. Karlsson, M. Carlsson Göthe, and M. Larsson, High-resolution inner-valence uv photoelectron spectra of the O_2 molecule and configuration-interaction calculations of ${}^2\Pi_u$ states between 20 and 26 eV, Phys. Rev. A **45**, 4374 (1992).
- [46] E. Andersson, M. Stenrup, J. H. D. Eland, L. Hedin, M. Berglund, L. Karlsson, A. Larson, H. Ågren, J.-E. Rubensson, and R. Feifel, Single-photon core-valence double ionization of molecular oxygen, Phys. Rev. A 78, 023409 (2008).
- [47] F. Frati, M. O. J. Y. Hunault, and F. M. F. de Groot, Oxygen K-edge x-ray absorption spectra, Chem. Rev. **120**, 4056 (2020).

- [48] N. Kosugi, J. Adachi, E. Shigemasa, and A. Yagishita, Highresolution and symmetry-resolved N and O K-edge absorption spectra of NO, J. Chem. Phys. 97, 8842 (1992).
- [49] J. Müller and H. Ågren, in *Proceedings of NATO ASI Conference on Molecular Ions*, edited by J. Berkowitz (Plenum, New York, 1980).
- [50] K. Huber and G. Herzberg, Molecular Structure and Molecular Spectra, IV. Constants of Diatomic Molecules (Van Nostrand Reinhold, New York, 1979).
- [51] A. Yagishita, E. Shigemasa, and N. Kosugi, Observation of Rydberg-valence mixing in high-resolution symmetry-resolved oxygen K-edge spectra of O₂, Phys. Rev. Lett. 72, 3961 (1994).
- [52] R. Püttner and K. Ueda, The angularly resolved O 1s ion-yield spectrum of O₂ revisited, J. Chem. Phys. **145**, 224302 (2016).
- [53] A. Lindblad, V. Kimberg, J. Söderström, C. Nicolas, O. Travnikova, N. Kosugi, F. Gel'mukhanov, and C. Miron, Vibrational scattering anisotropy in O₂-dynamics beyond the Born-Oppenheimer approximation, New J. Phys. 14, 113018 (2012).
- [54] H. Ågren and R. Arneberg, Origin of fine structure in the vicinity of the K-edges in the CO electron energy loss spectra, Phys. Scr. **30**, 55 (1984).
- [55] L. Cederbaum, A simple explanation of the breakdown of Koopmans' theorem for F₂ and N₂, Chem. Phys. Lett. 25, 562 (1974).
- [56] H. Ågren and H. Siegbahn, Semi-internal correlation in the auger electron spectrum of H₂O, Chem. Phys. Lett. 69, 424 (1980).
- [57] H. Ågren, On the interpretation of molecular valence Auger spectra, J. Chem. Phys. 75, 1267 (1981).
- [58] L. S. Cederbaum, J. Zobeley, and F. Tarantelli, Giant intermolecular decay and fragmentation of clusters, Phys. Rev. Lett. 79, 4778 (1997).